White-Emitting Conjugated Polymer Nanoparticles with Cross-Linked Shell for Mechanical Stability and Controllable Photometric Properties in Color-Conversion LED Applications

Eun-Ju Park, Talha Erdem, Vüsala Ibrahimova, Sedat Nizamoglu, Hilmi V. Demir,* and Dönüs Tuncel*

Departments of Chemistry, Physics, Electrical and Electronics Engineering, UNAM, National Nanotechnology Research Center, Institute of Materials Science and Nanotechnology, Bilkent University, Ankara 06800, Turkey

Water-soluble conjugated polymers have been receiving increasingly greater attention owing to their potential applications in the areas of biosensing, bioimaging, and optoelectronics. For example, they have been successfully utilized in the biosensor applications to detect proteins, nucleic acids, and sugars.[1-6] These polymers can be prepared by attaching ionic side groups to the polymer backbone. However, their synthesis is tedious and their solubility is still limited in the water. Good water solubility or dispersibility of the conjugated polymers can alternatively be achieved by converting them into nanoparticles.[7-13] Such water-dispersible conjugated polymer nanoparticles (CPNs) have been exploited in different applications. For example, Landfester, Sherf, List, and co-workers have demonstrated the use of CPNs in optoelectronic applications including light-emitting diodes and photovoltaics and also as inks in inkjet printing.[14-19] Foulger and co-workers demonstrated the use of hybrid conjugated polymer nanoparticles composed of blue- and green-emitting polymers in the construction of organic light-emitting diodes (OLEDs).[20] The color tuning of the electroluminescence for the devices was achieved through energy transfer. These nanoparticles have also been used in biological applications such as fluorescent images, biosensors, and oxygen sensors.[21-27] Apart from these applications, color tuning is important for the optoelectronic applications, especially for energy-efficient indoor and outdoor lighting.[28,29]

Water-dispersible conjugated polymer nanoparticles can be prepared mainly by

ABSTRACT We report on the synthesis and characterization of water-dispersible, mechanically stable conjugated polymer nanoparticles (CPNs) in shelled architecture with tunable emission and controllable photometric properties *via* cross-linking. Using a reprecipitation method, white-emitting polymer nanoparticles are prepared in different sizes by varying the concentration of polymer; the emission kinetics are tuned by controlling the shell formation. For this purpose, polyfluorene derivatives containing azide groups are selected that can be decomposed under UV light to generate very reactive species, which opportunely facilitate the inter- and intra-cross-linking of polymer chains to form shells. Nanoparticles before and after UV treatment are characterized by various techniques. Their size and morphologies are determined by using dynamic light scattering (DLS) measurements and imaging techniques including scanning electron microscopy (SEM) and atomic force microscopy (AFM). For optical characterization, UV—vis and steady-state and time-resolved fluorescent spectroscopies are performed. Solid-state behaviors of these CPNs are also investigated by forming films through drop-casting. Moreover, the photometric calculations are also performed for films and dispersions to determine the color quality. A device has been constructed to show proof-of-principle white light generation from these nanoparticles. Additionally, mechanical stability studies are performed and demonstrated that these nanoparticles are indeed mechanically stable by removing the solvent after cross-linking using a freeze-dryer and redispersing in water and THF. Optical and imaging data confirm that the redispersed particles preserve their shapes and sizes after cross-linking.

KEYWORDS: conjugated polymer nanoparticles · white light emission · cross-linked shell · color conversion

two methods, which are miniemulsion and reprecipitation. In the miniemulsion method, a two-phase system (oil-in-water) is used.[7,8] The polymer is dissolved in an organic solvent, which is not miscible with water, and added into a surfactant containing aqueous solution while sonicating. After the nanoparticle formation, the organic solvent is evaporated off to leave behind the conjugated nanoparticles stabilized by the surfactant. In the reprecipitation method, the polymer is dissolved in an organic
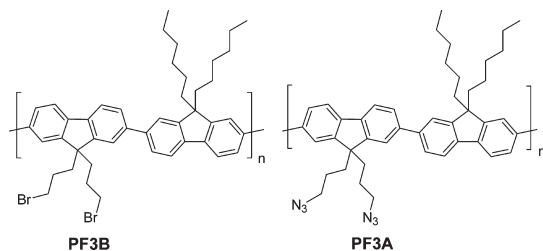
Chart 1. Molecular structures of poly[(9,9-dihexylfluorene)-*co-alt*-(9,9-bis(3-bromopropyl)fluorene)] (PF3B) and poly[-(9,9-dihexylfluorene)-*co-alt*-(9,9-bis(3-azidopropyl-)fluorene)] (PF3A).

PF3B   **PF3A**

solvent, which is a good solvent for the polymer and miscible with the water, and the solution is injected into a large volume of water while stirring rapidly. When the polymer chains are exposed to water, they fold into nearly spherical shapes to minimize the contact area. The organic solvent is removed to leave behind the conjugated polymer nanoparticles. This method does not require using surfactants or other additives and is conveniently very simple. A number of different conjugated polymers have been used for the formation of CPNs. However, the examples are mostly limited to highly hydrophobic conjugated polymers carrying no functional groups to be further modified. Although there are some recent examples involving the use of a capping agent that allows attaching CPNs to a biological entity,[30,31] the efforts are rather limited in developing stable CPNs without using capping agents, surfactants, and hydrophobes and exploring their applications in the area of optoelectronics. Another drawback preventing the exploitation of CPNs is the mechanical instability of these nanoparticles. To this end, the development of CPNs that are mechanically stable in water as well as in organic solvents and the surface functionalization of these CPNs are highly sought after for many applications.

RESULTS AND DISCUSSION

In this work, different than the previous reports, our idea was to prepare CPNs containing cross-linkable functional groups on the surface and then cross-linking these groups under light to create networks around the core forming shells. This has successfully served two purposes: (i) the cross-linked shells protect the nanoparticles, and mechanically stable CPNs are obtained in shelled architecture; and (ii) by cross-linking the shell, a core—shell structure is obtained in which the core and shell have different energy levels, with the core emitting in blue (donor) and the shell emitting in green-yellow (acceptor), and by controlling the shell formation, energy transfer between the donor core and acceptor shell can be tuned to generate white light. This provides us with the ability to make white-emitting, mechanically stable CPN luminophores with photometric properties controllable by design. To
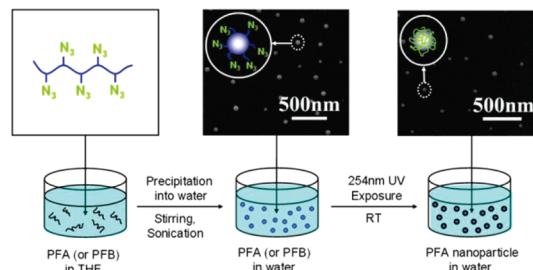

Figure 1. Cartoon representation of the conjugated polymer nanoparticle preparation.

study the modification of emission kinetics *via* the energy transfer in these core—shell CPNs, time-resolved experiments were conducted in solution and their lifetime analysis was carried out. Solid-state behaviors of these CPNs were also investigated by forming their films by drop-casting. Additionally, photometric calculations were performed in films to evaluate the color quality. Finally, a hybrid light-emitting diode (LED) has also been constructed from these nanoparticles by their integration on III-nitride LEDs for color conversion to demonstrate white light generation.

Synthesis of Conjugated Polymer Nanoparticles. To synthesize mechanically stable, water-dispersible conjugated polymer nanoparticles, we started with a polymer containing functional groups that allow for functionalization to achieve mechanical stability in the nanoparticles. For this purpose, we selected polyfluorene derivatives containing azide groups because azide groups can be decomposed under UV light to form very reactive species that facilitate the inter- and intra-cross-linking of polymer chains as we explained in our previous paper.[33] This polymer, namely, poly[(9,9-dihexylfluorene)-*co-alt*-(9,9-bis(3-azidopropyl)fluorene)] (PF3A) was prepared as reported previously.[32,33] Additionally, another polymer, namely, poly[(9,9-dihexylfluorene)-*co-alt*-(9,9-bis(3-bromopropyl)fluorene)] (PF3B), which contains bromide functional groups instead of azide, was prepared as reported previously (Chart 1).[32,33] This was used as the control polymer because the bromide group is less prone to decomposition, avoiding cross-linking, while azide strongly decomposes under UV—vis.

Light-emitting polymer nanoparticles were prepared in two different sizes using the reprecipitation method through tuning the concentration of polymer used. In this method, the polymer is dissolved in a good solvent (*e.g.*, THF) and precipitated into a poor solvent (*e.g.*, H$_2$O). Depending on the concentration of the polymer and the volume of the water used, the sizes of the nanoparticles are tuned. The size of the nanoparticles can be as small as a single chain containing a nanoparticle (Figure 1).

The size of these nanoparticles was determined as 170 and 50 nm from SEM images and 166 and 42 nm by DLS (Figure 2).

Photophysical Properties of Conjugated Polymer Nanoparticles before and after Cross-Linking. The cross-linking of
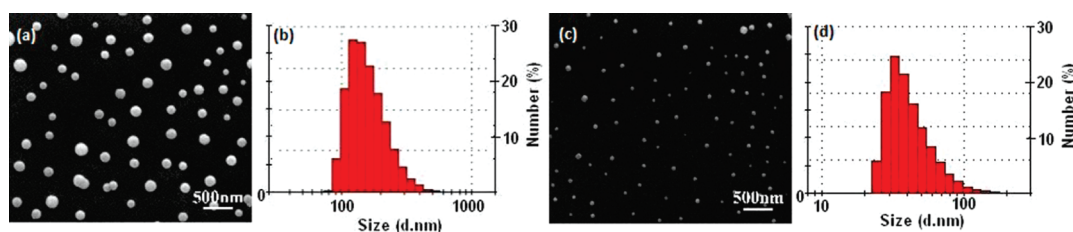
Figure 2. SEM images and DLS histograms of CPNs of PF3A: (a) large CPNs (PF3A-L NP), (b) DLS histogram of PF3A-L NPs and (c) small CPNs (PF3A-S NP), and (d) DLS histogram of PF3A-S NPs.
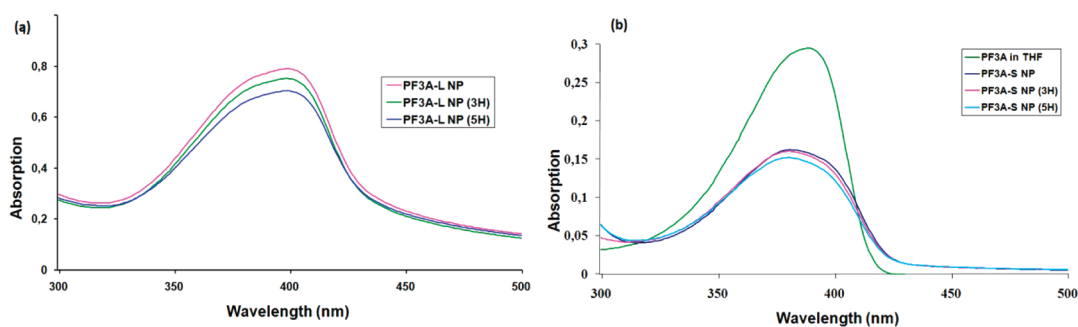

Figure 3. UV−vis spectra of PF3A in THF and CPN dispersion in water: (a) large nanoparticles (PF3A-L NP) and (b) small nanoparticles (PF3A-S NP) before and after UV exposure for 3 and 5 h in the air.

PF3A-large (PF3A-L) and PF3A-small (PF3A-S) nanoparticle dispersions in water was performed by using UV light at 254 nm over varying time scale at room temperature, and it was followed by UV−vis and fluorescence spectrometer over time. Two sets of cross-linking experiments were performed; one set of the experiments was carried out under air and the other set under nitrogen to take into account and study the possibility of the photo-oxidation.

Figure 3 shows the absorption spectra of PF3A-L and PF3A-S nanoparticle dispersion in water before and after cross-linking as well as the absorption spectrum of PF3A in THF (stock solution). Prior to nanoparticle formation, PF3A stock solution exhibits an absorption peak at 384 nm. However, upon nanoparticle formation, the absorption peak of PF3A-L appears at 398 nm, which is 14 nm red-shifted compared to stock solution of PF3A, and PF3A-S peak is seen at 379 nm, which is 5 nm blue-shifted. These results indicate that in the large nanoparticles (PF3A-L) there are chain−chain interactions, whereas in the case of small nanoparticles (PF3A-S), chain−chain interaction is limited and also there is a decrease in the conjugation length that can be attributable to the bending or twisting of the polymer backbone. The cross-linking procedure was followed by taking the UV−vis spectra of PF3A-L and PF3A-S. However, no significant changes were observed in the absorption spectra of the water dispersion of nanoparticles of PF3A-L and PF3A-S irrespective of the cross-linking time.

The fluorescence emission properties and the changes in the emission spectra after cross-linking were investigated using the fluorescence spectrometer.

PF3A-L shows a strong emission peak at 428 nm and vibronic bands at 451 and 480 nm (Figure 4). The emission peaks of nanoparticle dispersions in water red-shifted from 417 to 428 nm and from 442 to 451 nm compared to PF3A stock solution in THF. Large nanoparticles were exposed to 254 nm UV light over varying exposure times to achieve cross-linking. One set of experiments was conducted in air in the presence of oxygen, and the second set of experiments was carried out under nitrogen by degassing the nanoparticles with nitrogen for 30 min before UV exposure. As can be seen from the emission spectra of PF3A-L NP, UV exposure causes some changes in their spectra and a substantial decrease in the emission intensity of the PF3A-L NP.

The emission spectrum of PF3A-S NP shows a main peak at 423 nm and vibronic bands at 448 and 480 nm before cross-linking, which are approximately 5 nm red-shifted compared to the peaks of PF3A solution in THF (Figure 5). However, even after 1 h UV exposure, significant changes are observed in the emission spectrum of the nanoparticles. While the intensity of blue emission band decreases, a new broad band peaking at 530 nm and extending to 650 nm appears as observed in our previous study.[33] In both spectra of PF3A in air and under nitrogen (Figure 5a,b, respectively), the intensity of blue emission further decreases while the intensity of green emission increases with respect to blue emission and a gradual decrease in the overall emission intensity is observed with increasing exposure time.

The origin of the green emission in polyfluorene-based conjugated polymer has been investigated extensively and in general attributed to aggregate/
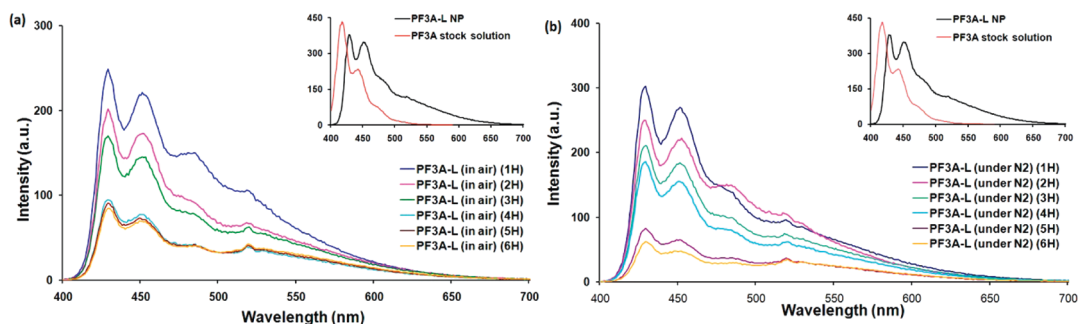
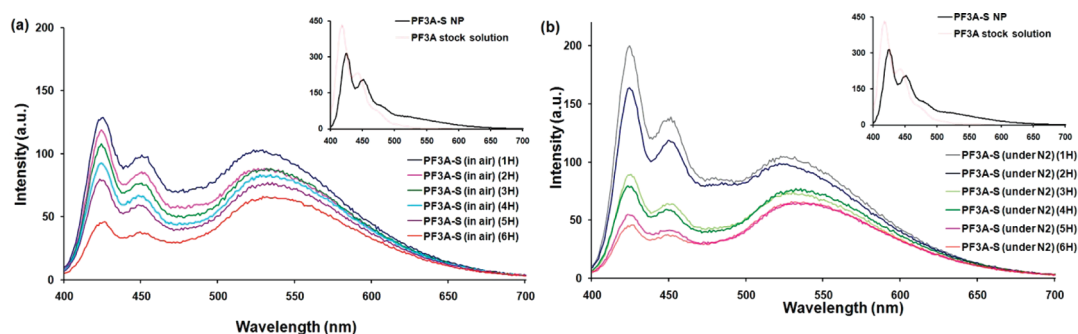**Figure 4.** Fluorescence spectra of PF3A-L NP after cross-linking (a) in the air and (b) under nitrogen.

Figure 5. Fluorescence spectra of PF3A-S after cross-linking (a) in the air and (b) under nitrogen.

excimer formation or keto defects.[34,35] However, we have shown in our previous paper that cross-linking *via* azide decomposition in the absence of oxygen, which is required for the keto defect formation, could still cause the emergence of the green emission band.[33] Azide groups can be decomposed under UV light to form very reactive nitrene species that facilitate the inter- and intra-cross-linking of polymer chains as well as might insert to the fluorene ring to create defects on the polymer backbone. However, there are no significant changes observed in the UV−vis spectra of nanoparticles upon UV exposure, while the emission spectra change; this suggest that the defects must be in minute quantity and have low molar absorptivity not to be seen in the UV−vis spectrum. These defects might have a low lying energy state that can act as an energy trap like in the fluorenone containing polymers;[34,35] consequently cross-linking most likely facilitates the excitation energy migration and energy transfer to the energy traps because the rotational freedom of polymer chains is greatly reduced upon cross-linking.

As can be seen, the changes in photoluminescence properties of small nanoparticles (PF3A-S) and large nanoparticles (PF3A-L) upon cross-linking differ substantially. These results indicate that the cross-linking has more effect on the small nanoparticles (PF3A-S) than the large nanoparticles (PF3A-L). The reason could be that the PF3A-L nanoparticles contain more polymer chains and are less tightly folded than the PF3A-S, and as a result, there will be more chain−chain

interactions, whereas PF3A-S nanoparticles consist of less polymer chains than the PF3A-L nanoparticles. In this case, the chain−chain interaction will be limited; this can also be seen from the UV spectra. Consequently, in the PF3A-L, the cross-linking will be inter-cross-linking of the polymer chains, while in PF3A-S, intrachain cross-linking will take place; this will in turn cause the formation of a rigid structure that can facilitate the excitation energy migration and energy transfer to the defects better than the less tightly cross-linked PF3A-L nanoparticles. The additional reason can also be explained by comparing the surface areas of small and large nanoparticles. Upon treating nanoparticles under UV light, the azide groups that are on the surface of the nanoparticles will be more readily available for the cross-linking than the azide groups buried inside a particle. In this case, the small nanoparticles have a greater surface area to volume ratio than the large nanoparticles.

Here, cross-linking serves two purposes; the first one is to form a network around the nanoparticle to protect the core from disintegration, or in other words, to achieve mechanical stability; and the second is for emission color tuning using one type of polymer and varying the cross-linking time. UV-light-triggered cross-linking assists the formation of a core−shell type of nanostructures in which a blue-emitting core and green-yellow-emitting shell can be obtained. Possibly due to an energy transfer from the blue core to the green-yellow shell (for which the time-resolved behavior provides supporting evidence), a broad band
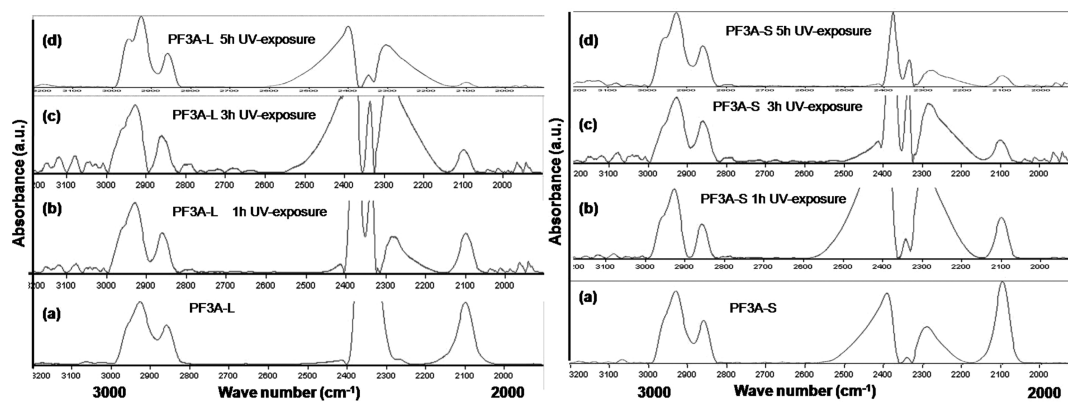
Figure 6. FT-IR spectra of PF3A-L (right panel) and PF3A-S (left panel) before (a) and after UV exposure for 1 h (b), 3 h (c), and 5 h (d). The large band around 2200−2500 cm^{-1} is due to CO_2.

covering the blue to yellow region of the visible spectrum generates white emission.

In order to investigate the extent of the azide decomposition and to gain insight for the structural changes in the polymer caused by azide decomposition, we recorded the FT-IR spectra of PF3A-S and PF3A-L nanoparticles over varying UV exposure time scales. The samples were prepared by concentrating nanoparticle dispersions and dropcasting onto silicon substrates; after drying the samples, IR spectra were recorded. Although noises probably due to scattering of nanoparticles made it difficult to obtain good quality FT-IR spectra, we were still able to extract some information on the azide (2100 cm^{-1}) and CH stretching (2820−2980 cm^{-1}) of the polymer because the bands of CH stretching as well as the azide band are quite strong (Figure 6). Since we would not expect CH stretching bands to decrease or increase upon UV exposure and we expect to see dramatic changes in the azide peak, we compared the intensity of CH stretching to the intensity of the azide peak of the small and large nanoparticles before and after UV exposure. As can be seen from the spectra, UV-exposed samples display a gradual decrease in the intensity of azide stretching peaks. However, even after 5 h UV exposure, some azide groups are still present. Comparing small nanoparticles to large nanoparticles by taking into account the intensity of azide bands to CH stretching peaks, there were no significant differences in the IR spectra.

In order to further investigate the probable structural changes caused by the decomposition of azide groups upon UV exposure, nanoparticles were prepared in D_2O and ^1H NMR spectra were recorded; however, in ^1H NMR spectrum, only some peaks due to aliphatic side chain protons were seen. Aromatic backbone protons were not detected because the mobility of the backbone is restricted upon folding in the nanoparticle formation. Some peaks of the aliphatic protons are seen because the side chains are more flexible. Thus, in this attempt, NMR experiments were not helpful for determining the structure of the nanoparticles after UV exposure.

The morphology of nanoparticles after cross-linking was also investigated by scanning electron microscopy (SEM) and dynamic light scattering (DLS). The SEM images and DLS measurement results indicate that there are no significant changes in the sizes of nanoparticles after cross-linking regardless of UV exposure time (Figures S1 and S2 and Table S1, Supporting Information). To study the mechanical stability, we also demonstrated that these nanoparticles are indeed mechanically stable by removing the solvent after cross-linking using a freeze-dryer and redispersing in water and THF again. Optical and imaging data confirmed that the redispersed particles appeared to preserve their shapes and sizes after cross-linking. As a control experiment in order to differentiate the effect of azide in the cross-linking process, PF3B-S nanoparticle dispersion in water was exposed to UV light using the same conditions used for the PF3A-based nanoparticles. The changes in the PL spectra over UV exposure time were followed again by fluorescence spectrometer. As can be seen from Figure S3 (Supporting Information), although there is a gradual decrease in the overall emission intensity, no significant changes are observed in the emission wavelengths even when the experiments were conducted in the presence of oxygen.

Time-resolved fluorescence (TRF) spectroscopy measurements were carried out for both types of the nanoparticle dispersions, and their corresponding lifetimes were calculated by an exponential reconvolution method. The results are summarized in Table 1. The lifetime analyses are made at 423 and 524 nm, which we consider as donor and acceptor wavelengths, respectively. In order to understand the effect of cross-linking on energy transfer, we took the particles cross-linked for 1 h as reference and compared these values with the ones belonging to CPNs cross-linked for 3 h, both in air and in N_2. For large and small NPs, the lifetimes at 423 nm are very short, on the order of a few tens of picoseconds. The effect of cross-linking on these lifetimes changes depending on the cross-link environment. UV exposure in air results in a decrease of the lifetime at this wavelength, whereas exposing the

TABLE 1. Lifetimes of Polymer Nanoparticle Dispersions

nanoparticles	lifetime at 423 nm (ns)	reduced χ^2	lifetime at 524 nm (ns)	reduced χ^2
PF3A-L (in air, 1 h)	0.039	0.856	3.991	1.007
PF3A-L (in air, 3 h)	0.012	1.036	4.304	1.030
PF3A-L (in N_2, 1 h)	0.029	0.875	5.111	1.121
PF3A-L (in N_2, 3 h)	0.060	0.966	4.599	0.950
PF3A-S (in air, 1 h)	0.106	1.167	4.924	0.944
PF3A-S (in air, 3 h)	0.029	1.679	5.112	0.957
PF3A-S (in N_2, 1 h)	0.107	0.998	5.286	0.957
PF3A-S (in N_2, 3 h)	0.272	1.105	3.028	0.976

nanoparticles to UV radiation under nitrogenized atmosphere increases the lifetime. We observe exactly the reversed relation at the acceptor wavelength. Cross-linking in air causes an increase in the lifetime, and cross-linking in N_2 decreases the lifetime at this wavelength, for both large and small nanoparticles.

In order to understand the nonradiative energy transfer mechanisms in these CPNs, these lifetime analyses are useful. From the decrease of donor lifetime, we can conclude that the cross-link increases the nonradiative energy transfer when carried out in air, for both large and small CPNs. However, cross-linking in a nitrogenized environment decreases the nonradiative energy transfer.

After investigating PF3A NP dispersions, their films were prepared with a drop-casting method. The fluorescence spectra of PF3A-L NP films are given in Figure 7a. This investigation reveals that all of the nanoparticle films keep their peak values in the dispersions. However, the intensity around the green spectral region is observed to weaken. This is especially effective for the cross-linked NP films. In addition, some relatively sharp peaks appear in the same wavelength interval, corresponding to the peak intensity wavelengths of the dispersions. This is considered not possibly to come from intrinsic material properties, as the material is essentially the same once the cross-linking is performed. This observation is attributed probably to the combined effects of the optical, environmental, and morphological changes as a result of casting the nanoparticles into a solid film on a quartz substrate.

The fluorescence spectra of the PF3A-S NP films are given in Figure 7b. As in the case of PF3A-L NPs, PF3A-S NPs show suppression of the green spectral range. However, the long wavelength components are still stronger than that of the PF3A-L NPs. An important point is the weakening of the vibronic band peak at *ca.* 450 nm for the films of cross-linked samples. In addition, sharp peaks are observed again as in the previous case. We do not expect such a spectral sharpening due to the intrinsic material of the nanoparticles. Instead, we think that this might probably be due to the film formation, in which an optical effect (*e.g.*, cavity effect) can be observed in conjunction with the possible environmental and morphological changes; however, we are still unable to make a conclusive statement to

distinctly identify the effect and work on understanding this observation.

Photometric Properties of Conjugated Polymer Nanoparticles before and after Cross-Link. Since the overarching objective of this work has been to generate white light with high quality using polymer nanoparticles, the quality of the general light was evaluated in an objective and quantitative way from the photometric point of view. The parameters that are most commonly used to quantify photometric performance include color rendering index (CRI), correlated color temperature (CCT), luminous efficacy of optical radiation (LER), and the ratio of the efficacies of scotopic to photopic vision (S/P). In addition, CIE 1931 chromaticity coordinates are used to characterize the operating color of the emission from these nanoparticles. Among them, CRI determines the ability of the luminophores to render the real colors of the illuminated objects. The best and poorest color renditions are expressed as 100 and −100, respectively. In order that a light source can be accepted to provide a good color rendition, CRI value needs to be larger than 80. Another important performance metric for the quality of white light is the correlated color temperature showing the temperature of the closest Planckian blackbody radiator to the chromaticity point of the luminophore. If the emitted color has a bluish tint, then the corresponding CCT increases, whereas the opposite happens when the emitted color shifts toward red.

Typically indoor lighting applications require low CCT levels (*i.e.*, CCT < 4000 K), which corresponds to warm white. Moreover, LER shows the optical efficiency of the emitted light as perceived by the human eye. For the artificial lighting application, an LER over 380 lm/W is highly desirable to compete with conventional light sources.[36] Furthermore, S/P expresses the ability of the white light to show the shape of the illuminated objects even under low optical power illumination conditions. Therefore, illuminants with high S/P values might be used for outdoor lighting applications. For that purpose, illuminants with S/P values larger than 2.5 are good candidates. In this work, our computations of CRI, LER, and S/P are undertaken according to ref 37 and CCT calculation is made using the method developed in ref 38 by disregarding values larger than 250 000 K. The *x* and *y* chromaticity coordinates are calculated using the CIE 1931 standard colorimetric observer data.

Since the drop-casted films exhibit significant deviations from the dispersion spectra in the green region, it is meaningful to investigate only PF3A-S NP films in terms of photometric performance due to their wider spectrum to obtain high performance. The required calculations are therefore done only for these NP films, and the results are presented in Table 2. Here note that, although calculation of CRI is attempted, the results show that it is not possible to find a meaningful quantity. To calculate a reasonable CRI, a reference
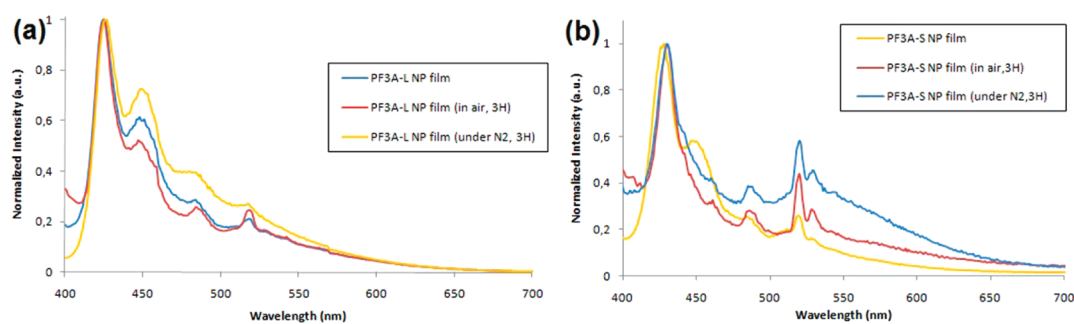
Figure 7. Fluorescence spectra of the films prepared from (a) PF3A-L NP and (b) PF3A-S NP dispersions.

spectrum depending on the CCT of a reference light source should be found. The color distance between (u,v) chromaticity points of the emission spectrum under test and the reference needs to be less than 0.005 in order for the calculation to be meaningful. However, for the polymer nanoparticles, the color emitted lies toward the blue, and the resulting value becomes very high and a reasonable CCT value cannot be found. As a result, a proper reference spectrum cannot be assigned for them, and therefore, CRI cannot be calculated. Reasonable CCT values for the polymer nanoparticle films cannot be obtained due to the dominant blue content in the emission spectrum. Since Planckian locus converges to a single point on the chromaticity as the temperature increases, emitters with very dominant blue content have either very high CCTs or their CCTs cannot be determined at all. All of these nanoparticle films have a very dominant emission within the bluish region; as a result, a reasonable CCT cannot be assigned.

Among other important performance criteria, LER is the one that reveals the efficiency of the color emitted by making use of the sensitivity characteristics of the human eye. According to the results presented in Table 2, all of the nanoparticle films remain inefficient under photopic vision (for environments illuminated with high optical powers) when they are not cross-linked. However, cross-linking nanoparticles improves LER compared to the non-cross-linked ones. In addition, cross-linking under inert atmosphere results in further increase of LER. This increase stems from the increased overlap of the photoluminescence spectrum of the film with the sensitivity curve of the human eye. However, to compete with the conventional light sources, the spectral content in the green-yellow and in red needs to further increase. Investigation of the S/P reveals that all of these nanoparticle films have very high S/P values. These high values are caused by better overlap between the scotopic eye sensitivity curve and illuminant spectrum. By making use of these light sources, very effective sources can be developed for outdoor lighting application under scotopic vision conditions (for the environments illuminated with low optical power).

TABLE 2. Results of the Photometric Calculations

sample	CCT (K)	LER (lm/W)	S/P	x	y
PF3A-S NP film	N/A	137	5.32	0.1820	0.1363
PF3A-S NP film (3 h, in air)	N/A	195	3.64	0.2144	0.2152
PF3A-S NP film (3 h, in N$_2$)	N/A	209	3.47	0.2209	0.2299

The photoluminescence spectra of the dispersions are depicted in Figure 4 and Figure 5 and were investigated in previous sections. In this section, we are investigating the photometric performance of these dispersions. The photometric computation results are given in Tables S2 and S3 in Supporting Information for the cases of cross-linking large (PF3A-L) and small (PF3A-S) nanoparticles, respectively. Although CRI is calculated for all of the dispersion spectra, no result is obtained due to the lack of having a good reference spectrum.

Investigation of PF3A-L NP Dispersions. The CCT values of PF3A-L NPs cannot be calculated for the cases of cross-linking for 6 h. This behavior can be explained by considering the dominance of blue color in the spectrum as can be understood from the chromaticity coordinates. CCT can be determined only when cross-linking is continued over 6 h. As the cross-linking duration increases, the relative green-yellow content of the spectra increases. As a result of this, LER values increase and S/P values decrease. Furthermore, it is also observed that performing the cross-linking under N$_2$ increases the relative green-yellow content in the spectra, leading to higher LER and lower S/P values when compared to the cross-linking in air. Although an improvement is observed from the perspective of photometric performance as the cross-linking period is increased and when the cross-linking environment is deoxidized, the performance of the dispersions still remains decent. In addition to that, the intensity of the emission decreases as the cross-linking duration increases.

Investigation of PF3A-S NP Dispersions. Similar to the case of PF3A-L NPs, cross-link time and the ratio of green-yellow to the blue spectral content are proportional. As a result of this, S/P decreases whereas LER increases. Because the green-yellow spectral content in PF3A-S NPs is more dominant compared to that of the
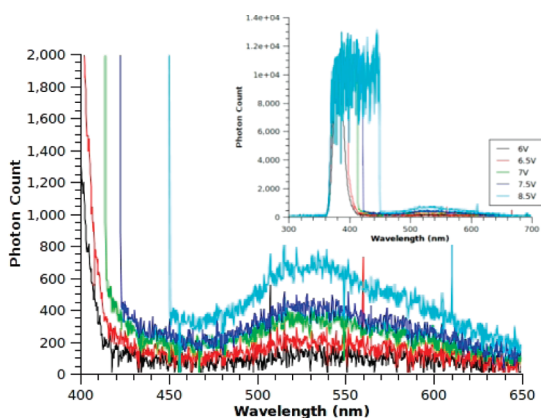
Figure 8. Emission spectrum of PF3A-S nanoparticle integrated n-UV LED electrically driven under different biases.

PF3A-L NPs, even with a cross-link time of 1 h, CCT can be calculated. Cross-linking under N_2, however, causes more dominant blue content compared to cross-linking in air. As a result of this, CCT and S/P values get higher and LER values become lower when cross-linking is made under inert atmosphere. It is also worth mentioning that LER values of the illuminants can be increased up to 350 lm/W by increasing the cross-link time, while preserving relatively higher S/P values. Cross-linking allows for tuning these photometric properties.

Cross-Linked Conjugated Polymer Nanoparticle Integrated LED. The thin films of PF3A-S NPs are excited with an n-UV LED. The IV characteristics of the n-UV LED and its emission spectrum are as shown in Figure S4 (see Supporting Information). The spectrum of the PF3A-S nanoparticles excited by n-UV LED is also depicted in Figure 8. As expected, the resulting spectrum closely follows the photoluminescence spectrum of the films. However, the peak at around 420 nm is not easily resolvable. This is due to the relatively broad full width at half-maximum (fwhm) of the LED at the required voltage levels to pump the nanoparticles.

These results show that PF3A-S nanoparticles can be used as white luminophores that cover a significant interval of the visible region. The CIE 1931 chromaticity coordinates of the spectra are (0.28, 0.34), (0.27, 0.33), (0.26, 0.31), (0.24, 0.23), and (0.20, 0.10) at 6, 6.5, 7, 7.5, and 8.5 V, respectively. As an another indicator of this blue shift in the spectrum, correlated color temperature values increase by increasing the applied voltage, except for the case at 7.5 V. They are 8125, 9325, 11 337,

34 463, and 34 366 K at 6, 6.5, 7, 7.5, and 8.5 V, respectively. These values show that, by using these polymer nanoparticle luminophores, cool white light sources are generated by controlling the cross-link time. Color rendering index of these sources is also calculated. However, due to the impossibility of finding a good reference source, which is a drawback of the CRI method, a reasonable quantity can be found only for 7.5 V case. The resulting value comes out to be 66.35, showing a moderate color rendering performance. As a result, here we demonstrate cool white light sources having moderate color rendering performance by integrating PF3A-S nanoparticles on a n-UV LED.

CONCLUSIONS

In this work, we described the synthesis, characterization, and application of functional group containing white-emitting conjugated polymer nanoparticles (CPNs) based on the polyfluorene derivatives in various sizes and tunable emission wavelength and photometric properties. Within the framework of this paper, we have shown that PF3A CPNs can be prepared from a functional group containing conjugated polymers for further modification, and functional groups do not prevent nanoparticle formation. Depending on the polymer concentrations and the volume of the water used, nanoparticles can be prepared in desired sizes. Cross-linking experiments were carried out both in air and under nitrogen. The results show that large CPNs have shown little changes in the PL spectra over the exposure time, while small nanoparticles have exhibited significant changes in the spectra over time. For small nanoparticles, we observed that a new emission band occurs spanning the wavelengths of 500–650 nm accompanied with the decreased intensity in the blue region due to the larger surface area containing cross-linkable functional groups. Furthermore, no significant change has been found in morphology and size upon cross-linking. In addition, we demonstrated that these CPNs are mechanically stable after light-triggered cross-linking of the azide functional group. We also showed that light sources designed from these nanoparticles have high correlated color temperature and high S/P value, which corresponds to high efficiency under low optical power levels. Finally, we demonstrated a proof-of-concept conjugated polymer nanoparticle integrated color-conversion LED to show their use as luminophores in lighting applications.

EXPERIMENTAL SECTION

Materials. All of the reagents were purchased from the Sigma-Aldrich Chemical Co. and were used as received. 2, 7-Dibromo-9,9-bis(3-bromopropyl)-9H-fluorene was synthesized according to our previous reports.[32,33]

Poly[(9,9-dihexylfluorene)-co-alt-(9,9-bis(3-bromopropyl)fluorene)] (PF3B). PF3B was synthesized using the similar procedure as previously reported.[32,33] However, in this synthesis, 2,7-dibromo-9,9-bis(3-bromopropyl)-9H-fluorene was used: yield 57%; ^{1}H NMR (400 MHz, CDCl$_3$, δ) 7.70 (m, 8H, Ar H), 7.86 (m, 4H, Ar H),

3.22 (br, 4H, $-CH_2Br$), 2.32 (m, 4H, CH_2), 2.18 (m, 4H, CH_2), 1.15 (m, 18H, CH_2), 0.81 (m, 6H, $-CH_3$); gel permeation chromatography (GPC) $M_n = 0.5 \times 10^4$ g mol^{-1}, $M_w = 1.4 \times 10^4$ g mol^{-1} (THF was used as a solvent and polystyrene as standard).

Poly[(9,9-dihexylfluorene)-co-alt-(9,9-bis(3-azidopropyl)fluorene)] (PF3A). PF3A was synthesized by treating PF3B with NaN_3 in DMF as in the previous report: yield 90%; ^{1}H NMR (400 MHz, CDCl$_3$, δ) 7.70 (m, 8H, Ar H), 7.86 (m, 4H, Ar H), 3.10 (br, 4H, CH_2Br), 2.40 (m, 4H, CH_2), 2.13 (m, 4H, CH_2), 1.16 (m, 18H, CH_2), 0.81 (m, 6H, CH_3); gel permeation chromatography (GPC) $M_n = 0.6 \times 10^4$ g mol^{-1}, $M_w = 1.6 \times 10^4$ g mol^{-1} (THF was used as a solvent and polystyrene as standard).

Nanoparticle Preparation. Conjugated polymer nanoparticles were prepared in two different sizes. Ten milligrams of polymer was dissolved in 10 mL of THF and stirred overnight. The solution was made up to volume of 100 mL by adding THF, and subsequently it was filtered through a 0.45 μm syringe filter.

CPNs with Average Sizes of 166 nm by DLS. Eight milliliters of this stock solution was injected rapidly into 40 mL of water while stirring using a sonicator. The dispersion of nanoparticles was sonicated further for 20 min and stirred additionally another 30 min using a magnetic stirrer. THF was removed under reduced pressure; the resulting nanoparticle dispersion was filtered through a 0.45 μm syringe filter.

CPNs with Average Sizes of 42 nm by DLS. The procedure is the same but here 2 mL of polymer stock solution was injected into 100 mL of water to prepare CPNs.

General. The morphology of nanoparticles before and after cross-linking was investigated with a scanning electron microscope (SEM, Quanta 200 FEG SEM). Samples were prepared by dropping dispersions of PF3A-L and PF3A-S onto freshly cleaved silicon wafer without coating with Pt. Dynamic light scattering (DLS, Zetasizer Nano-ZS) measurements were carried out at a wavelength of 633 nm using laser as the light source at room temperature. The time-dependent autocorrelation function of the scattered light intensity was measured at an angle of 90°. The average particle diameters were calculated by Marquardt method. The DLS measurements were usually repeated at least three times, and the average values were reported. The UV–vis spectra were recorded on a CARY UV–vis spectrophotometer. Fluorescence measurements were carried out on a CARY Eclipse fluorescent spectrophotometer equipped with a xenon lamp excitation source. Milli-Q water (18.2 MΩ) was used for the preparation of nanoparticles.

To obtain relatively strong photoluminescence from the films, the dispersions of polymer nanoparticles were concentrated to increase the number of particles per unit area in the film. The films were prepared by drop-casting 25 μL of the concentrated dispersions of non-cross-linked nanoparticles (denoted as PF3A-S NP-film), of the nanoparticles cross-linked for 3 h in air (denoted as PF3A-S NP-film (3 h, in air)), and of the nanoparticles cross-linked for 3 h under nitrogen (denoted as PF3A-S NP-film (3 h, under N$_2$)). Drying of these films was then carried out under vacuum. The photoluminescence spectra were obtained by using Varian Cary Eclipse fluorescence spectrophotometer by exciting the nanoparticles at 380 nm. Lifetime measurements are taken using FluoTime 200 of PicoQuant at an excitation wavelength of 375 nm.

Near-UV light-emitting diode (n-UV LED) was fabricated from InGaN/GaN quantum well epitaxy by making use of metal oxide chemical vapor deposition (MOCVD) such that its peak emission wavelength was located at 378 nm. The thin film of PF3A-S NPs was prepared by drop-casting. The emission spectra were collected by an Ocean Optics integrating sphere.

Supporting Information Available: SEM images of PF3A-L and PF3A-S NPs before and after cross-linking, fluorescence spectra of PF3B stock solution, PF3B-S NP dispersions before and after cross-linking in the air, DLS results of cross-linked nanoparticle PF3A-L, PF3A-S, and PF3B-S in air, photometric computation results of PF3A-L and PF3A-S dispersions for different cross-linking durations. This material is available free of charge *via* the Internet at http://pubs.acs.org.

REFERENCES AND NOTES

1. Pu, K.-Y.; Liu, B. Optimizing the Cationic Conjugated Polymer-Sensitized Fluorescent Signal of Dye Labeled Oligonucleotide for Biosensor Applications. *Biosens. Bioelectron.* **2009**, *24*, 1067–1073.
2. McQuade, D. T.; Pullen, A. E.; Swager, T. M. Conjugated Polymer-Based Chemical Sensors. *Chem. Rev.* **2000**, *100*, 2537–2574.
3. Dore, K.; Dubus, S.; Ho, H. A.; Levesque, I.; Brunette, M.; Corbeil, G.; Boissinot, M.; Boivin, G.; Bergeron, M. G.; Boudreau, D.; *et al.* Fluorescent Polymeric Transducer for the Rapid, Simple, and Specific Detection of Nucleic Acids at the Zeptomole Level. *J. Am. Chem. Soc.* **2004**, *126*, 4240–4244.
4. Liu, B.; Dan, T. T. T.; Bazan, G. C. Collective Response from a Cationic Tetrahedral Fluorene for Label-Free DNA Detection. *Adv. Funct. Mater.* **2007**, *17*, 2432–2438.
5. Miranda, O. R.; You, C. C.; Phillips, R.; Kim, I. B.; Ghosh, P. S.; Bunz, U. H. F.; Rotello, V. M. Array-Based Sensing of Proteins Using Conjugated Polymers. *J. Am. Chem. Soc.* **2007**, *129*, 9856–9857.
6. Disney, M. D.; Zheng, J.; Swager, T. M.; Seeberger, P. H. Detection of Bacteria with Carbohydrate-Functionalized Fluorescent Polymers. *J. Am. Chem. Soc.* **2004**, *126*, 13343–13346.
7. Tuncel, D.; Demir, H. V. Conjugated Polymer Nanoparticles. *Nanoscale* **2010**, *2*, 484–494.
8. Landfester, K. Miniemulsion Polymerization and the Structure of Polymer and Hybrid Nanoparticles. *Angew. Chem., Int. Ed.* **2009**, *48*, 4488–4507.
9. Landfester, K. The Generation of Nanoparticles in Miniemulsions. *Adv. Mater.* **2001**, *13*, 765–768.
10. Landfester, K.; Montenegro, R.; Scherf, U.; Günther, R.; Asawapirom, U.; Patil, S.; Neher, D.; Kietzke, T. Semiconducting Polymer Nanospheres in Aqueous Dispersion Prepared by a Miniemulsion Process. *Adv. Mater.* **2002**, *14*, 651–655.
11. (a) Wu, C.; Szymanski, C.; McNeill, J. Preparation and Encapsulation of Highly Fluorescent Conjugated Polymer Nanoparticles. *Langmuir* **2006**, *22*, 2956–2960. (b) Wu, C.; Szymanski, C.; Cain, Z.; McNeill, J. Conjugated Polymer Dots for Multiphoton Fluorescence Imaging. *J. Am. Chem. Soc.* **2007**, *129*, 12904–12905.
12. (a) Huyal, I. O.; Ozel, T.; Tuncel, D.; Demir, H. V. Quantum Efficiency Enhancement in Film by Making Nanoparticles of Polyfluorene. *Opt. Express* **2008**, *16*, 13391–13397. (b) Ozel, I. O.; Ozel, T.; Demir, H. V.; Tuncel, D. Non-radiative Resonance Energy Transfer in Bi-polymer Nanoparticles of Fluorescent Conjugated Polymers. *Opt. Express* **2010**, *18*, 670–684.
13. Baykal, B.; Ibrahimova, V.; Er, G.; Bengü, E.; Tuncel, D. Dispersion of Multi-walled Carbon Nanotubes in an Aqueous Medium by Water Dispersible- Conjugated Polymer Nanoparticles. *Chem. Commun.* **2010**, *46*, 6762–6764.
14. Piok, T.; Gamerith, S.; Gadermaier, C.; Plank, H.; Wenzl, F. P.; Patil, S.; Montenegro, R.; Kietzke, T.; Nehrer, D.; Scherf, U.; *et al.* Organic Light-Emitting Devices Fabricated from Semiconducting Nanospheres. *Adv. Mater.* **2003**, *15*, 800–804.
15. Kietzke, T.; Nehrer, D.; Landfester, K.; Montenegro, R.; Güntner, R.; Scherf, U. Novel Approaches to Polymer Blends Based on Polymer Nanoparticles. *Nat. Mater.* **2003**, *2*, 408–412.
16. Kietzke, T.; Nehrer, D.; Kumke, M.; Montenegro, R.; Landfester, K.; Scherf, U. A. Nanoparticle Approach To Control the Phase Separation in Polyfluorene Photovoltaic Devices. *Macromolecules* **2004**, *37*, 4882–4890.
17. Piok, T.; Plank, H.; Mauthner, G.; Gamerith, S.; Gadermaier, C.; Wenzl, F. P.; Patil, S.; Montenegro, R.; Bouguettaya, M.; Reynolds, J. R.; *et al.* Solution Processed Conjugated Polymer Multilayer Structures for Light Emitting Devices. *Jpn. J. Appl. Phys.* **2005**, *44*, 479–484.
18. Fisslthaler, E.; Sax, S.; Scherf, U.; Mauthner, G.; Moderegger, E.; Landfester, K.; List, E. J. W. Inkjet Printed Polymer Light-Emitting Devices Fabricated by Thermal Embedding of

ARTICLE

Semiconducting Polymer Nanospheres in an Inert Matrix. *Appl. Phys. Lett.* **2008,** *92*, 183305.

19. Fisslthaler, E.; Blümel, A.; Landfester, K.; Scherf, U.; List, E. J. W. Printing Functional Nanostructures: A Novel Route towards Nanostructuring of Organic Electronic Devices *via* Soft Embossing, Inkjet Printing and Colloidal Self Assembly of Semiconducting Polymer Nanospheres. *Soft Matter* **2008,** *4*, 2448–2453.

20. Huebner, C. F.; Roeder, R. D.; Foulger, S. H. Nanoparticle Electroluminescence: Controlling Emission Color through Förster Resonance Energy Transfer in Hybrid Particles. *Adv. Funct. Mater.* **2009,** *19*, 3604–3609.

21. Howes, P.; Thorogate, R.; Green, M.; Jickells, S.; Daniel, B. Synthesis, Characterisation and Intracellular Imaging of PEG Capped BEHP-PPV Nanospheres. *Chem. Commun.* **2009,** 2490–2492.

22. Green, M.; Howes, P.; Berry, C.; Argyros, O.; Thanou, M. Simple Conjugated Polymer Nanoparticles as Biological Labels. *Proc. R. Soc. A* **2009,** *465*, 2751–2759.

23. Wu, C.; Bull, B.; Christensen, K.; McNeill, J. Ratiometric Single-Nanoparticle Oxygen Sensors for Biological Imaging. *Angew. Chem., Int. Ed.* **2009,** *48*, 2741–2745.

24. Moon, J. H.; Deans, R.; Krueger, E.; Hancock, L. F. Capture and Detection of a Quencher Labeled Oligonucleotide by Poly(phenylene ethynylene) Particles. *Chem. Commun.* **2003,** 104–105.

25. Moon, J. H.; MacLean, P.; McDaniel, W.; Hancock, L. F. Conjugated Polymer Nanoparticles for Biochemical Protein Kinase Assay. *Chem. Commun.* **2007,** 4910–4912.

26. Moon, J. H.; McDaniel, W.; MacLean, P.; Hancock, L. E. Live-Cell-Permeable Poly(*p*-phenylene ethynylene). *Angew. Chem., Int. Ed.* **2007,** *46*, 8223–8225.

27. Rahim, N. A. A.; McDaniel, W.; Bardon, K.; Srinivasan, S.; Vickerman, V.; So, P. T. C.; Moon, J. H. Conjugated Polymer Nanoparticles for Two-Photon Imaging of Endothelial Cells in a Tissue Model. *Adv. Mater.* **2009,** *21*, 3492–3496.

28. Erdem, T.; Nizamoglu, S.; Sun, X. W.; Demir, H. V. A Photometric Investigation of Ultra-efficient LEDs with High Color Rendering Index and High Luminous Efficacy Employing Nanocrystal Quantum Dot Luminophores. *Opt. Express* **2010,** *18*, 340–347.

29. Phillips, J. M.; Coltrin, M. F.; Crawford, M. H.; Fischer, A. J.; Krames, M. R.; Mueller-Mach, R.; Mueller, G. O.; Ohno, Y.; Rohwer, L. E. S.; Simmons, J. A.; *et al.* Research Challenges to Ultra-efficient Inorganic Solid-State Lighting. *Laser Photon. Rev.* **2007,** *1*, 307–333.

30. Howes, P.; Green, M.; Bowers, A.; Parker, D.; Varma, G.; Kallumadil, M.; Hughes, M.; Warley, A.; Brain, A.; Botnar, R. Magnetic Conjugated Polymer Nanoparticles as Bimodal Imaging Agents. *J. Am. Chem. Soc.* **2010,** *132*, 9833–9842.

31. Howes, P.; Green, M.; Bowers, A.; Levitt, J.; Suhling, K.; Hughes, M. Phospholipid Encapsulated Semiconducting Polymer Nanoparticles: Their Use in Cell Imaging and Protein Attachment. *J. Am. Chem. Soc.* **2010,** *132*, 3989–3996.

32. Huyal, I. O.; Ozel, T.; Koldemir, U.; Nizamoglu, S.; Tuncel, D.; Demir, H. V. White Emitting Polyfluorene Functionalized with Azide Hybridized on Near-UV Light Emitting Diode for High Color Rendering Index. *Opt. Express* **2008,** *16*, 1115–1124.

33. Huyal, I. O.; Koldemir, U.; Ozel, T.; Demir, H. V.; Tuncel, D. On The Origin of High Quality White Light Emission from a Hybrid Organic/Inorganic Light Emitting Diode Using Azide Functionalized Polyfluorene. *J. Mater. Chem.* **2008,** *18*, 3568–3574.

34. Romaner, L.; Pogantsch, A.; De Freitas, P. S.; Scherf, U.; Gaal, M.; Zojer, E.; List, E. J. W. The Origin of Green Emission in Polyfluorene-Based Conjugated Polymers: On-Chain Defect Fluorescence. *Adv. Funct. Mater.* **2003,** *13*, 597–601.

35. Zhao, W.; Cao, T.; White, J. M. On the Origin of Green Emission in Polyfluorene Polymers: The Roles of Thermal Oxidation Degradation and Crosslinking. *Adv. Funct. Mater.* **2004,** *14*, 783–790.

36. Schubert, E. F. *Light-Emitting Diodes*; Cambridge University Press: New York, 2006.

37. Wyszecki, G.; Stiles, W. S. *Color Science: Concepts and Methods, Quantitative Data and Formulae*; Wiley: New York, 1982.

38. Robertson, A. R. Computation of Correlated Color Temperature and Distribution Temperature. *J. Opt. Soc. Am.* **1968,** *58*, 1528–1535.